Athens Journal of Technology and Engineering - Volume 12, Issue 3, September 2025 – Pages 195-210

Internal Model Principle-based Control for Sinusoidal Disturbance Rejection in Field-Oriented Control

By Ibrahim Allafi & Lyndon Brown±*

This research presents results of combining the field-oriented control of motors with a more general Internal Model Principle controller rather than the specific case of integral control. The goal is to have a motor that can remove narrow band disturbances without impacting its performance outside of this specific frequency. This research is motivated by eliminating tremors in human limbs. We verify our approach by initially implementing the algorithm in Matlab and then conducting experimental trials in our lab using two brushless DC motors. The first motor (Motor 1) will generate a sinusoidal torque signal on the shaft, while the second motor (Motor 2) will utilize our algorithm to cancel this torque. Both motors are connected by a coupler. When Motor 1 initiates rotation with a sinusoidal torque signal, Motor 2 driven with our algorithm will freeze the motion in Motor 1. Thus, the torque on Motor 2 will match that of Motor 1. We then add additional broadband torque in Motor 1 and show that Motor 2 can still match the sinusoidal torque while ignoring this additional movement. We will investigate the difference between using the encoders from both motors as the driving signal for our control algorithm.

Keywords: *internal model principle, field-Oriented Control, disturbance rejection, brushless DC motors, tremor signal*

Introduction

The challenge of disturbance cancellation arises in numerous applications, such as active noise and vibration control, optical stabilization in laser communication systems, vibration management in space structures due to control moment gyroscopes, helicopter vibration reduction, and tension regulation in paper machines (Pigg & Bodson 2009). Rotating mechanical systems like magnetic disk drives (Brown & Zhang 2004) and CD players often experience periodic disturbances (Pigg & Bodson 2011).

Two methods are suggested for rejecting sinusoidal disturbances. The first method is an indirect approach, where the frequency of the disturbance is estimated, and then the control law's magnitude and phase are adjusted accordingly based on this estimated frequency. The second method is a direct approach, which simultaneously estimates and cancels the disturbance frequency using a phase-locked loop (Bodson & Douglas 1997). Brown and Zhang (2004) introduce an algorithm designed to eliminate periodic disturbances with uncertain frequencies. This algorithm employs an internal model structure with an adaptive frequency component, which operates alongside a stabilizing controller. In Pigg and Bodson (2009), the challenge of

*PhD Student, Western University, Canada.
±Associate Professor, Western University, Canada.

https://doi.org/10.30958/ajte.12-3-4 doi=10.30958/ajte.12-3-4

disturbance rejection is addressed for plants with unknown and time-varying characteristics. The algorithm by Pigg and Bodson (2009) utilizes online estimates of the plant's frequency response and disturbance parameters to tackle this issue. Pigg and Bodson (2013) suggest an algorithm that relies on an adaptive harmonic steady-state and a magnitude phase-locked loop to cancel disturbances of uncertain frequencies affecting an unknown plant. On the other hand, Pigg and Bodson (2011) introduced a novel algorithm for estimating frequencies using a two-phase induction motor model, effectively rejecting disturbances of unknown frequencies.

Recent progress in disturbance rejection methods has introduced new strategies to handle sinusoidal disturbances in mechanical systems. Kamaldar and Hoagg (2021) presented adaptive harmonic control algorithms, both centralized and decentralized, which use discrete Fourier transform data to counteract known-frequency sinusoidal disturbances in systems with multiple inputs and outputs. Wen and Yan (2020) proposed a control method based on disturbance prediction, using an additional observer to forecast and reject unknown sinusoidal disturbances, improving the stability of systems with time delays. R. Madonski and colleagues (2020) developed a robust control algorithm within the active disturbance rejection control framework, including a tool to estimate harmonic disturbance frequencies, and showed its effectiveness through tests on torsional systems. Lastly, Long (2021) investigated a switched internal model approach to manage sinusoidal disturbances in nonlinear switched systems, focusing on improving adaptability and maintaining robust performance.

One of the applications that experiences multiple harmonic sinusoidal disturbances is the parkinsonian hand tremor. In Zhou et al. (2016), the characteristics of finger and wrist tremors were described. They identified that the frequencies of the first, second, and third harmonics of resting tremors across all joints were found to be between 3.5 Hz to 5.8 Hz, 6.9 Hz to 11.5 Hz, and 10.4 Hz to 17.3 Hz, respectively. The postural tremor's first to third harmonics fall between 3.9 Hz to 7.7 Hz, 7.7 Hz to 11.2 Hz, and 11.5 Hz to 16.8 Hz, respectively. In the tremor suppression device, our attention is solely directed towards suppressing involuntary motion, with no need to address voluntary motion. In Zhou et al. (2018), a method to suppress tremor signals was introduced, building upon the data provided in Zhou et al. (2016a). Their system comprises of sensors, actuation components, and a control system. IMU sensors are utilized to measure tremors at the wrist and joints of the fingers (specifically the thumb and index finger). The actuation system incorporates three brushless DC (BLDC) motors, each controlled by a commercial motor controller. Extracting the voluntary signal from the measured signal is essential for controlling the motion of patients' fingers and wrists. The effectiveness of the control system heavily relies on the accuracy of the tremor estimator, thus emphasizing the need for precise tremor estimation. In their study, they employed the Weighted-frequency Fourier Linear Combiner (WFLC) to estimate the tremor signal from the measurement signal before it is sent to the BLDC motor. The WFLC methodology was introduced by Riviere et al. (1998) and Veluvolu et al. (2007).

In Zhou et al. (2016b), the authors demonstrated the design and validation of a High-Order Weighted-Frequency Fourier Linear Combiner-based Kalman Filter for estimating parkinsonian tremors. They utilized the frequency tracking capability of two WFLCs, complemented by a Kalman Filter for better amplitude estimation. The results showed that the proposed algorithm had better tremor estimation performance than the WFLC. Additionally, the results highlighted the significant impact of the order of the Parkinsonian tremor model used in the Kalman Filter on estimation performance. However, This method was complicated for estimating the tremor signal from voluntary motion.

This motivates us to improve the control system to cancel specific frequencies within the bandwidth. Why is this study necessary? Based on previous research in tremor signal suppression, the goal is to suppress the tremor signal, defined as a sinusoidal signal, without affecting voluntary motion, which is defined as a non-sinusoidal signal. In this paper, we will test the Internal Model Principle (IMP) for rejecting periodic signals within a specific bandwidth. The algorithm relies on Field-Oriented Control (FOC) to generate torque signals (disturbances) on the shaft of a BLDC motor, which is then connected to another motor controlled by IMP and a common controller such as a PID controller or a lead-lag compensator.

This paper is organized as follows: the first section was an introduction that prefaced the topic of sinusoidal disturbances and their cancellation. The second section provides a brief literature review on BLDC motors. The third section details the setup of the experiment to control the torque on BLDC Motor 1 using FOC. The fourth section presents the design of the controller based on the experimental results using IMP to cancel disturbances in a specific bandwidth. In the fifth section the designed controller will be utilized to control Motor 2 to freeze Motor 1 or eliminate the fundamental frequency when we add the first harmonic to the disturbance signal. The sixth section presents the results and discussion. Finally, the seventh section concludes the paper and future works.

Literature Study of BLDC Motor

BLDC motors have evolved over the past 25 years through the integration of a compact motor, such as a permanent magnet stepper motor, with a rotor position sensor and an electronic switching circuit. Referred to as BLDC motors, they operate on DC power without the need for commutators and brushes. The fundamental elements of a BLDC motor consist of a permanent magnet rotor, a stator with windings comprising three, four, or more phases, a rotor position sensor, and an electronic control circuit to control the phases of the rotor winding.

BLDC motors have many advantages like being efficient, reliable, low-maintenance, quieter than brushed DC motors, and capable of high-speed operation. However, they can be pricier than regular DC motors because they use permanent magnets and need more complex controls (Edition & Chapman 2012).

In this study, we aim to control the torque of a BLDC motor to stop or reduce the rotation of the motor's shaft without causing any damage. Relying solely on voltage control may not provide the precise control required and could potentially damage the motor when attempting to stop it abruptly. We utilized FOC to control the torque of the BLDC motor. FOC involves adjusting the direct axis current (i_d) and the quadrature axis current (i_q) to achieve the desired torque (r_d). Further details about FOC can be found in Kronberg (2012), Sharma and Sindekar (2016), and Fadli et al. (2019). Figure 1 shows the FOC algorithm.

Figure 1. *Block Diagram of FOC*

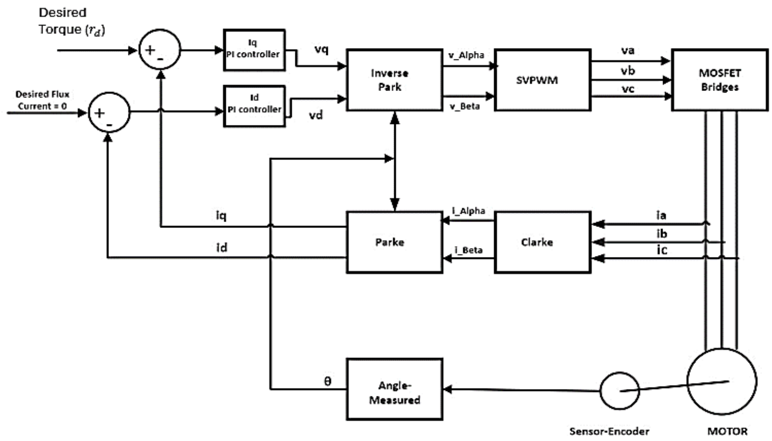

Experimental Setup For Torque Control

In this section, we present the required equipment needed to control the torque of BLDC Motor 1 based on the FOC algorithm. Figure 2 illustrates the setup of the system in the lab. The necessary equipment includes:

1) Microcontroller: The microcontroller used in this experiment is the STM32F446RE, shown in Figure 2. Developed by STMicroelectronics and based on the ARM Cortex-M4 core, it operates at a clock frequency of up to 180 MHz, providing high processing power. Additionally, the resolution of its analog-to-digital converters and digital-to-analog converters is 12 bits.
2) Motor Driver: In this experiment, we utilized the DRV8302 motor driver, developed by Texas Instruments, as shown in Figure 2. This driver requires a power supply of 24 V and a maximum current of 2 A. Additionally, the motor driver offers essential functions for motor control, including high and low side gate drivers, current sensing, and protection features.
3) BLDC Motor: The motor was used to control its torque or generate torque signals on its shaft. It has the following specifications: a rated voltage of 24 V, input power of 15 Watts, maximum speed of 480 RPM, and maximum torque of 2 Kg·cm. Additionally, this motor is equipped with two sensors: an encoder with a resolution of 4096 pulses per revolution and a Hall effect sensor.
4) AC/DC Adapter: The adapter was used to supply power to the motor driver. It has a maximum voltage and current of 24 V and 2 A respectively.

Figure 2. *Experimental Configuration for Torque Control: (A) STM32F446RE, (B) Motor Driver DRV8302, (C) BLDC Motor*

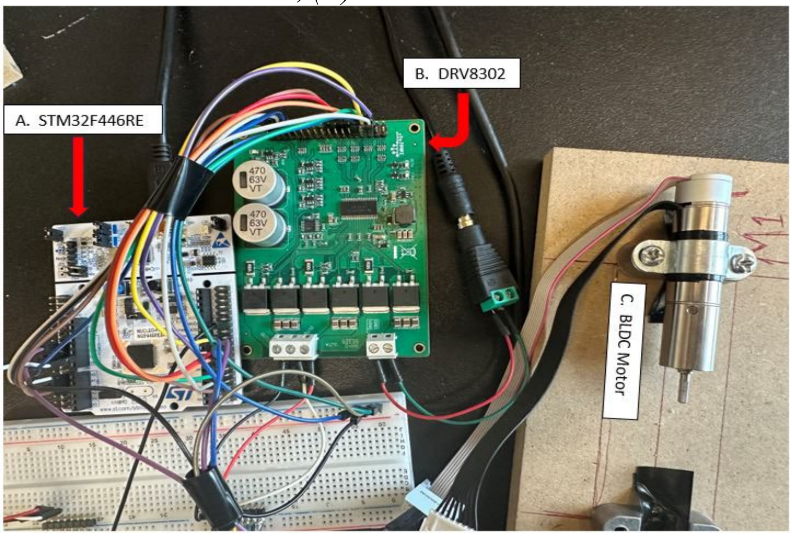

Deriving PI Control Parameters

The setup used to control the torque on the BLDC motor's shaft was connected as displayed in Figure 2. To achieve a desired torque (r_d) close to the actual torque (i_q), it is important to determine the PI controller parameters for the quadrature current (i_q) and direct current (i_d) accurately.

The Ziegler-Nichols method was employed for this purpose. This method aims to find the parameters of the PID controller through trial and error. The procedure involves initially setting the I and D gains to zero. Then, the P gain is gradually increased until it reaches a critical value, known as K_{cr}, at which the loop output begins to oscillate. The values of K_{cr} and the oscillation period, P_{cr}, are then used to adjust the gains accordingly (Erol et al. 2017).

$$K_p = 0.45K_{cr} \qquad T_i = \frac{P_{cr}}{1.2} \tag{1}$$

Results from Torque Controller

From the Ziegler-Nichols technique, the parameters of the PI controller were determined as in Table I. In this experiment, we applied those parameters to control the torque circuit. The desired torque is set to increase from 0.05 A to 0.5 A and remain at 0.5 A for a period of time, then drop to 0.2 A and remain at that level for another period of time. No load was placed on the shaft.

Table 1. *PI Parameters*

Parameter	PI for i_d	PI for i_q
K_{cr}	22	44
P_{cr}	0.0629 s	0.06269 s
K_P	10	20
T_i	0.0522 s	0.0522 s

Figure 3 shows a comparison between the desired torque and the actual torque on the shaft. The black line represents the applied torque on the motor, while the red line shows the actual torque on the motor. It can be observed that the actual torque on the motor closely matched the applied torque. Additionally, the current on each phase (I_a, I_b, I_c) of the BLDC motor was measured, as shown in Figure 4. The maximum amplitude of each phase corresponded to the actual torque of the motor, and the angle between each phase was 120^o. This indicates that the torque applied to the motor was the desired torque.

Figure 3. *Controlling Torque in BLDC Motor Using FOC Algorithm*

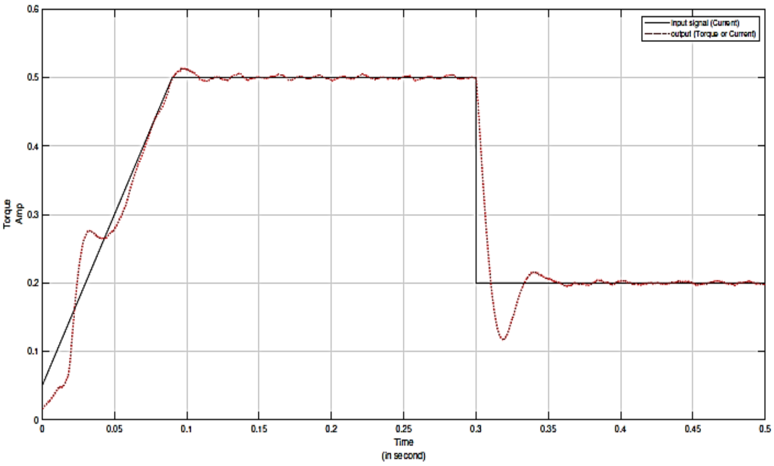

Figure 4. *Three-Phase Currents and Actual Torque of the BLDC Motor*

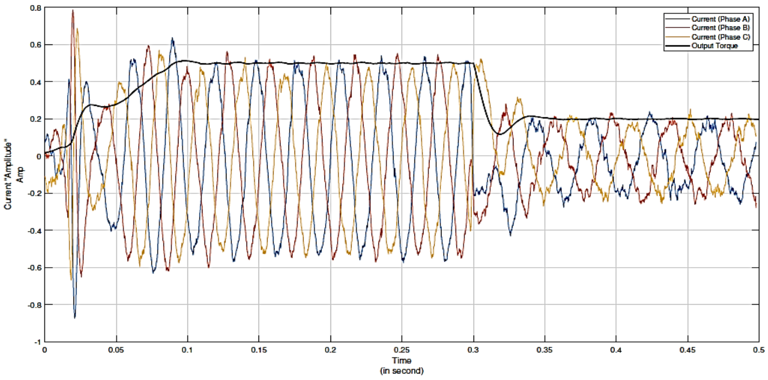

Determine the Transfer Function between the desired and the Actual Torque

We need to find the transfer function that describes how the desired torque relates to the actual torque. This will help us design the controller for controlling BLDC Motor 2 in the next step. In control engineering, the system identification technique is commonly used to establish the transfer function of a model. This method deals with black-box models of dynamical systems, where inputs and outputs can be measured (Ljung 2001). Based on this study, we can determine the transfer function since we have both input and output data. Upon observing Figure 3, we notice that the transfer function will be of second degree due to the presence of one overshoot. The second-degree transfer function is represented as follows:

$$H(s) = \frac{K_{DC} * \omega_n}{s^2 + 2\zeta\omega_n s + {\omega_n}^2} \quad (2)$$

$$K_{DC} = \frac{y(\infty)}{r(\infty)} \quad (3)$$

$$M_P = \frac{y(t_P) - y(\infty)}{y(\infty)} \quad (4)$$

$$\zeta = \sqrt{\frac{ln^2(M_P)}{ln^2(M_P) - \pi^2}} \quad (5)$$

$$\omega_n = \frac{\pi}{t_P\sqrt{1-\zeta^2}} \quad (6)$$

In the equations, K_{DC} represents the steady-state gain, denoted as the DC gain. Here, $y(\infty)$ and $r(\infty)$ represent the DC values of the output and input, respectively. Additionally, M_P denotes the overshoot, t_P stands for the peak time, while ω_n represents the natural radian frequency, and ζ signifies the damping ratio.

When utilizing the system identification method to determine the parameters of the transfer function, the values of K_{DC}, ζ and ω_n are found to be 1, 0.37 and 192.11 rad/sec, respectively. The transfer function between desired torque and actual torque is:

$$\frac{i_q}{r_d} = \frac{3.691X10^4}{s^2 + 142.6s + 3.691X10^4} \quad (7)$$

We validated the accuracy of the transfer function using Matlab by applying the same input signal as shown in Figure 3. Figure 5 represents a comparison between the motor's response and the output of the transfer function. Both outputs demonstrate an identical response, confirming the validity of the transfer function.

Figure 5. *Comparison of Desired Torque and Actual Torque from Motor with Transfer Function*

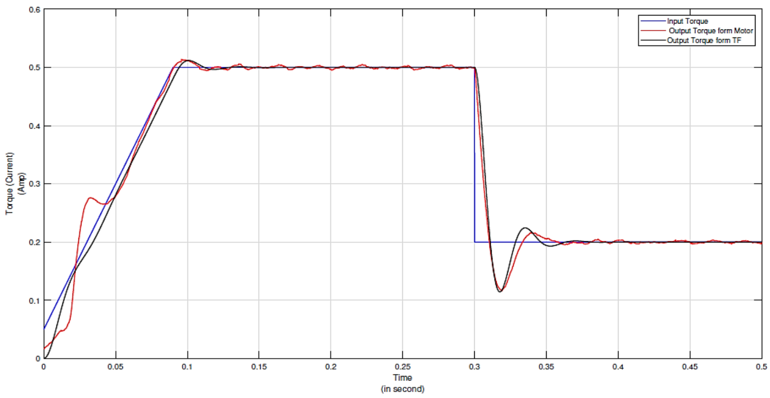

The Proposed Technique Based on IMP

The IMP, developed by Francis and Wonham in 1976, is a well-known approach for reducing periodic disturbances in control systems. In a feedback system, the IMP aims to introduce closed-loop transmission zeros that counterbalance the critically stable poles linked to disturbance and/or reference signals (Francis & Wonham 1976). In Mohsen, Brown and Chen (2017), the authors introduce a new tuning approach for an adaptive IMP based signal identification algorithm. The algorithm was designed with a bandpass filter with notches at specific frequencies within the bandwidth of the filter. Based on this study, we aim to cancel the disturbance signal within a narrow bandwidth without an effect on others. Figure 6 shows the block diagram of the controller utilized for canceling specific frequencies of the disturbance signal.

Figure 6. *Control System Architecture*

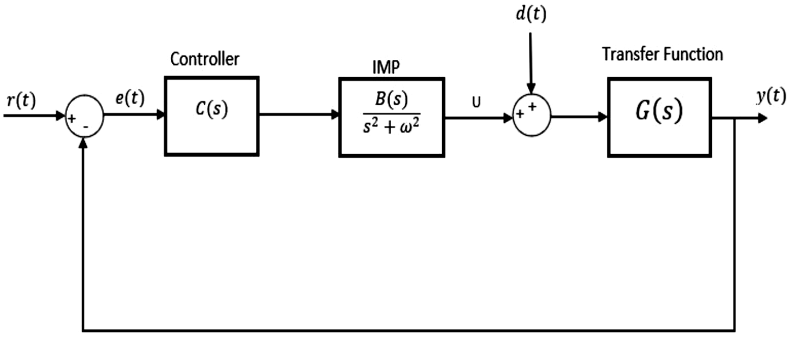

From the third section, we determined the transfer function representing the relationship between input torque and actual torque. Therefore, G(s) corresponds to the transfer function as defined in Equation 7. In the IMP, the numerator B(s) takes the form $s + \omega$, where ω denotes the frequency targeted for cancellation. Meanwhile, C(s) denotes a generic controller, such as a P Controller, PI Controller, PID Controller, or lead lag compensator. In this study, C(s) is configured as the P controller with P = 5.

The closed-loop transfer function from d(t) to y(t) in Figure 6 will be represented by the following equation:

$$\frac{Y(S)}{D(s)} = \frac{G(s)}{1 + C(s)G(s)IMP(S)} \tag{8}$$

We assume there is a sinusoidal disturbance signal given by $d(t) = 0.7\sin\,(2\pi x 1t)$. Since we do not need to track any signal, the reference signal r(t) is set to zero. We choose ω in the IMP to match the disturbance frequency, and we plot the Bode diagram of the closed-loop transfer function for Equation 8. Figure 7 shows the Bode plot.

Figure 7. *Bode Plot of the Transfer Function* $\frac{Y(S)}{D(s)}$

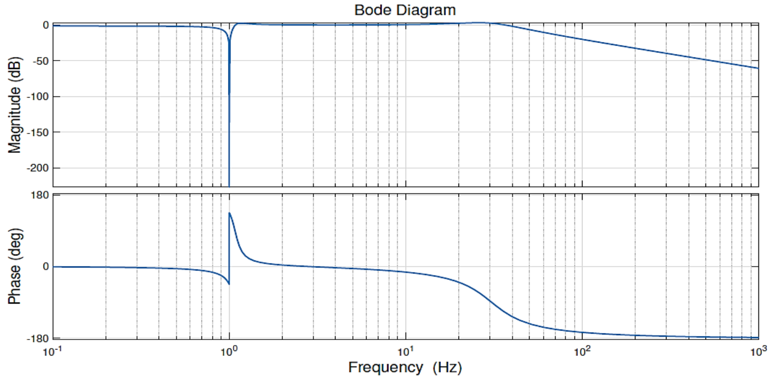

Based on the frequency response analysis, the system behaves as a low-pass filter with a cutoff frequency of approximately 40 Hz, where the magnitude plot decreases by -3 dB from its peak value. Within this specific bandwidth, the algorithm should cancel the disturbance at the frequency ω specified by the IMP and disregard other frequencies.

Simulation Result and Discussion

If the disturbance comprises a single frequency, the algorithm will effectively suppress it. The algorithm's response to this disturbance is illustrated in Figure 8. However, if an additional harmonic is added, it falls within the bandwidth shown in Figure 7. Consequently, the disturbance transforms into $d(t) = 0.7\sin(2\pi x 1t) + 0.3\sin(2\pi x 2t)$.

Figure 8. *Algorithm Response at Single Frequency*

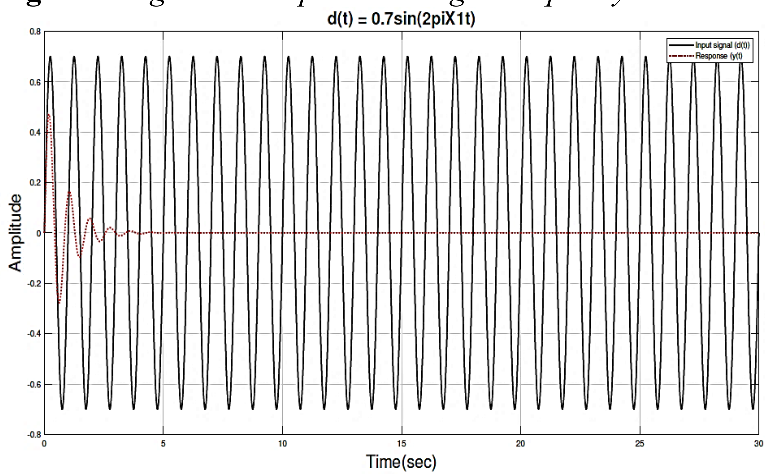

Figure 9 illustrates the response to a disturbance signal containing a harmonic. The black wave represents the disturbance signal with a fundamental frequency of one Hz and a harmonic at two Hz. The red wave shows the actual response. The outcome demonstrates cancellation of the fundamental frequency, while the first harmonic appears in the response with the same frequency and amplitude. This simulation showcases the ability to cancel specific frequencies while ignoring others, as long as they fall within a specified bandwidth. In the next section, we will validate these findings experimentally.

Figure 9. *Algorithm Response at Fundamental Frequency and its First Harmonic*

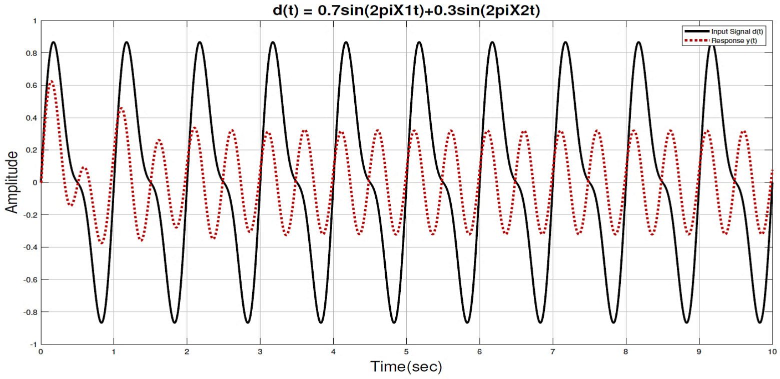

Experimental Validation: A Practical Study

In this section, we introduce the experimental configuration comprising an extra motor (Motor 2), a motor driver, and a microcontroller. These elements have similar the specifications to those used in the torque control experiment discussed in the third section. Figure 10 illustrates the experimental setup on the bench-top. In this experiment, we have two circuits: the torque control circuit, which produces disturbances on the shaft of Motor 1, and the control circuit for disturbance cancellation. We applied the algorithm explained in the fourth section to regulate the speed of Motor 2. Two motors are connected by a coupler. The torque circuit represents as an open loop control system relative to the disturbance cancellation circuit.

Figure 10. *Visualization of the Experimental Setup – Showing Two Circuits (A. Control Torque Circuit) and (B. Control Circuit for Disturbance Cancellation*

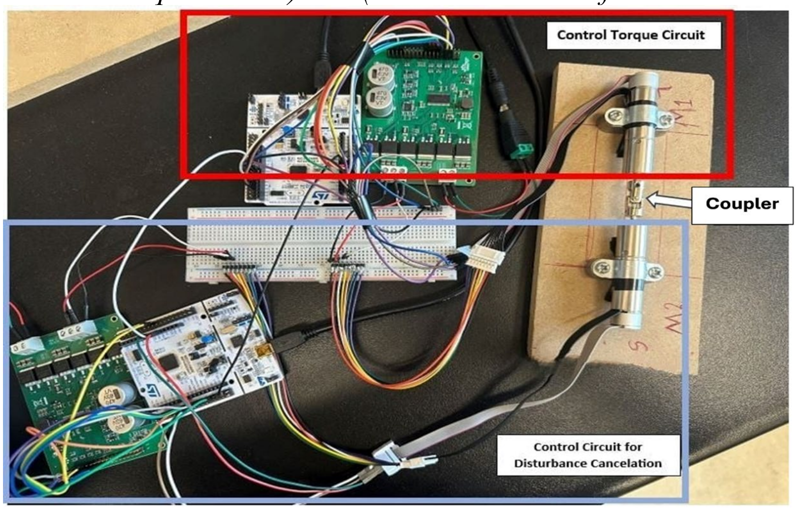

The aim of this experiment is to assess whether the angular velocity of Motor 2 synchronizes with that of Motor 1 when a sinusoidal torque is applied to Motor 1, with the disturbance cancellation circuit deactivated. Additionally, we investigate whether activating the disturbance cancellation circuit allows Motor 2 to freeze Motor 1 in the presence of a fundamental frequency disturbance or to eliminate the harmonic frequency when the disturbance includes both the fundamental and first harmonic.

Results and Discussion

For further clarification, the results of the experiment are divided into two sections: Section A examines the scenario where only a sinusoidal torque signal with the fundamental frequency is applied to Motor 1, representing a disturbance signal on Motor 2. In Section B, a first harmonic is added to the sinusoidal torque signal applied to Motor 1, also acting as a disturbance signal on Motor 2.

A. Results for Fundamental Frequency Disturbance

We applied a sinusoidal torque signal to Motor 1, containing only the fundamental $r_d(t) = 0.7\sin(2\pi x 1t)$. Then, we measured the angular velocities of both Motor 1 and Motor 2 with the controller algorithm for Motor 2 turned off. The results indicate that when Motor 1 initiates rotation due to torque applied at one Hz, the shaft of Motor 2 also begins to rotate, matching the angular velocity of Motor 1. Upon measuring the angular velocity of both motors, it was observed that the frequency was nearly one Hz. Figure 11 illustrates the comparison of angular velocities between the two motors. The black waveform represents the measured angular velocity from Motor 1, while the red waveform represents that from Motor 2.

Figure 11. *Comparison of Angular Velocities between Motor 1 and Motor 2 without the Cancellation Algorithm*

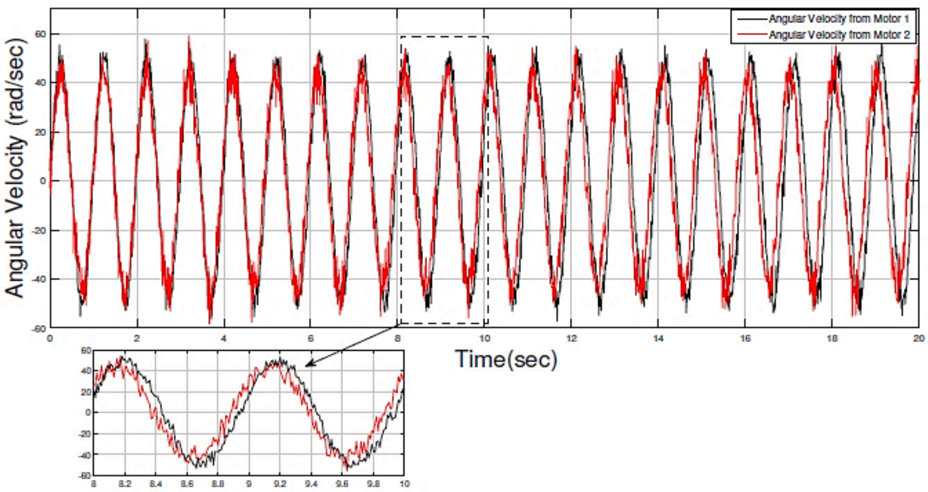

After investigation, it was determined that Motor 2 can replicate the angular velocity of Motor 1. Upon activating the cancellation circuit's algorithm, Motor 2 can freeze Motor 1. The results illustrated in Figure 12 show that the angular velocity of Motor 1, represented by the red waveform, decreases to zero. This indicates that the cancellation algorithm effectively freezes Motor 1.

Figure 12. *Measurement of Angular Velocity from Motor 1 before (Black Waveform) and after (Red Waveform) Cancellation*

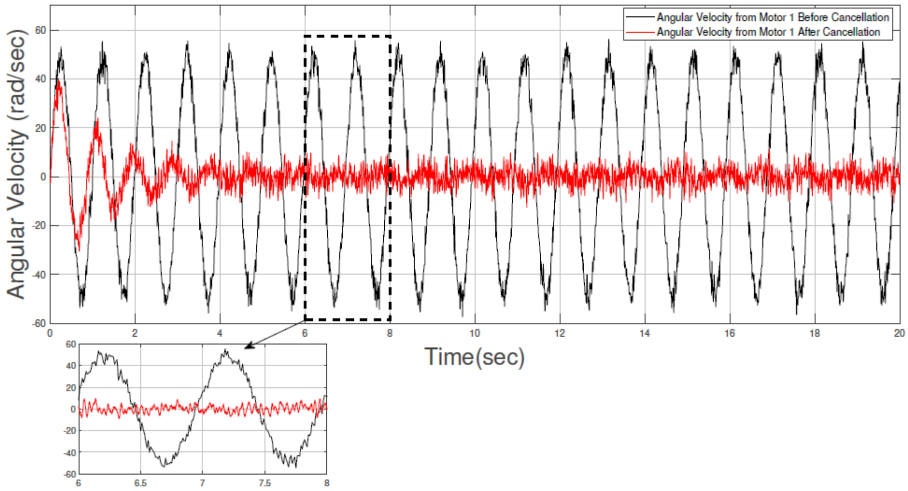

B. Results for the Disturbance with a Fundamental Frequency and First Harmonic

We added a first harmonic to the torque signal applied to Motor 1 $r_d(t) = 0.7\sin(2\pi x 1t) + 0.3\sin(2\pi x 2t)$. Figure 13 displays the angular velocities measured by the encoders of Motor 1 (illustrated in black waveform) and Motor 2 (illustrated in red waveform) when the disturbance cancellation circuit was inactive. Analyzing the measurement signal using FFT, as shown in Figure 14, identified two frequency components: a fundamental frequency and its first harmonic, that corresponds to the applied torque frequency signal.

Figure 13. *Comparison of Angular Velocities between Motor 1 and Motor 2 without the Cancellation Algorithm when First Harmonic is Added*

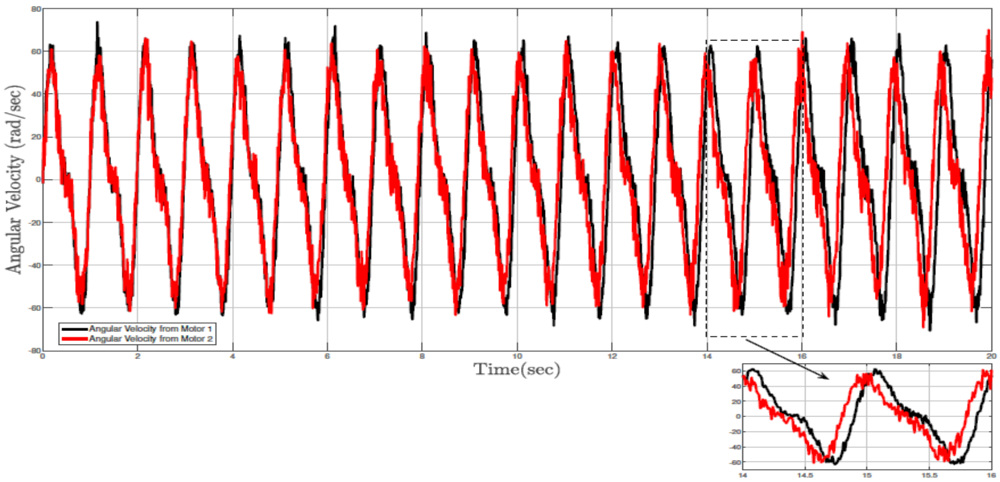

Figure 14. *Visualization of the FFT of Angular Velocity Data Obtained from Motor 1 and Motor 2 before Cancellation*

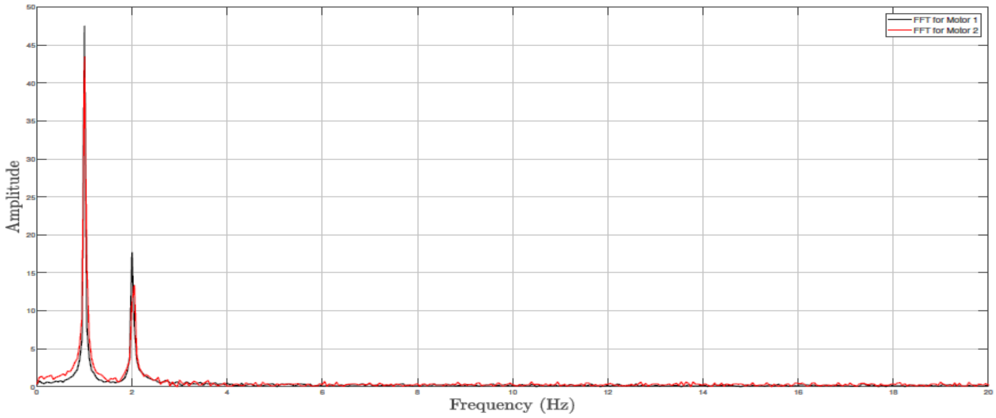

When the cancellation circuit's algorithm was activated, Motor 2 began to suppress the fundamental frequency, as shown in Figure 15. However, Motor 1 did not stop completely; it continued to rotate at the frequency of the first harmonic of the applied torque signal. Additionally, analyzing the FFT of the output signal from Motor 1 after the cancellation circuit was activated showed that the remaining frequency was two Hz. This equals the first harmonic of the applied torque shown in Figure 16.

Figure 15. *Angular Velocity Measurements from Motor 1 before (Black Waveform) and after (Red Waveform) Activation of Cancellation when First Harmonic is Added*

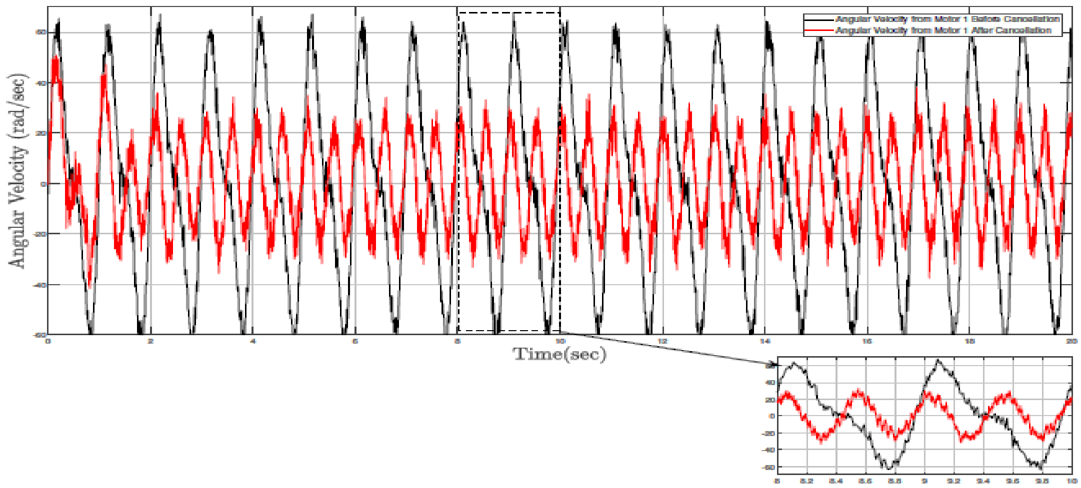

Figure 16. *Visualization of FFT of Angular Velocity Data Obtained from Motor 1 after Cancellation*

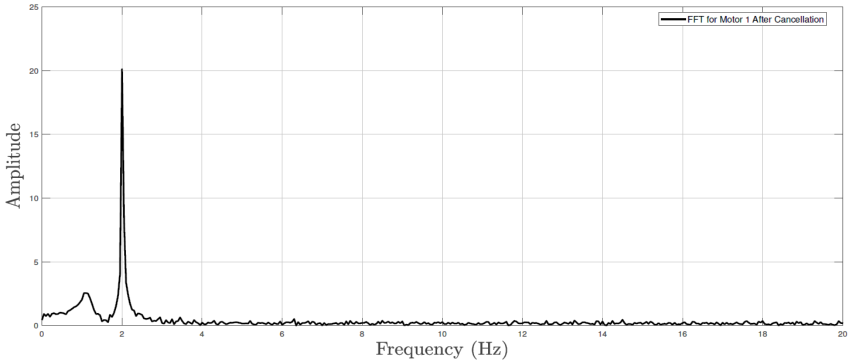

Conclusion and Future Work

This work proposes the implementation of a system to cancel sinusoidal disturbance signals within a narrow bandwidth. The objective of this research was to eliminate a specific frequency without affecting other frequencies within the same bandwidth. The study combines FOC of motors with the IMP. The simulation results demonstrated the ability to cancel a specific frequency within a given bandwidth without impacting other frequencies.

In the experimental setup, two motors were used to implement the proposed algorithm. Motor 1 was controlled by FOC to control torque on its shaft, simulating the introduction of a disturbance. Motor 2, controlled by the proposed IMP-based algorithm, aimed to cancel the unwanted frequencies generated by Motor 1. The experimental results illustrated that Motor 2 could successfully cancel the targeted frequency while leaving other frequencies unaffected, validating the effectiveness of the proposed approach in practical applications.

Future work will concentrate on the development of advanced algorithms for the cancellation of sinusoidal disturbance signals through the on-line tuning of the parameters of the controller in real time. This will involve defining the narrow bandwidth to effectively eliminate the targeted frequencies within that range. The aim is to enhance the precision and robustness of frequency cancellation while maintaining the integrity of non-targeted frequencies within the specified bandwidth.

References

Bodson M, Douglas SC (1997) Adaptive algorithms for the rejection of sinusoidal disturbances with unknown frequency. *Automatica* 33(12): 2213–2221.

Brown LJ, Zhang Q (2004) Periodic disturbance cancellation with uncertain frequency. *Automatica*, 40(4): 631–637.

Edition F, Chapman SJ (2012) Electric machinery fundamentals.

Erol O, Aktaş M, Altun Y (2017) Obtaining of PI control parameters for vector controlled PMSM. In *Proc. Int. Conf. Hydraul. Pneum. Tools, Seal. Elem. Fine Mech. Specif. Electron. Equip. Mechatronics*.

Fadli MR, Musyasy MM, Furqani J, Purwadi A (2019, November) Modelling of field orientation control (FOC) method in 120 kW brushless DC motor (BLDC). In *2019 6th International Conference on Electric Vehicular Technology (icevt)*, 383–389. IEEE.

Francis BA, Wonham WM (1976) The internal model principle of control theory. *Automatica* 12(5): 457–465.

Kamaldar M, Hoagg JB (2021) Centralized and decentralized adaptive harmonic control for sinusoidal disturbance rejection. *Control Engineering Practice* 112: 104814.

Kronberg A (2012) Design and simulation of field oriented control and direct torque control for a permanent magnet synchronous motor with positive saliency. Available at: https://www.semanticscholar.org/paper/Design-and-Simulation-of-Field-Oriented-Control-and-Kronberg/35d4381596d336c6802148cdd7674551fe7f1d32.

Ljung L (2001, May) Black-box models from input-output measurements. In *IMTC 2001. Proceedings of the 18th IEEE instrumentation and measurement technology conference. Rediscovering measurement in the age of informatics (Cat. No. 01CH 37188)*. Vol. 1, 138–146). IEEE.

Long L (2021) Global disturbance rejection of switched nonlinear systems with switched internal model. *Journal of Systems Science and Complexity* 31(1): 161–172.

Madonski R, Stanković M, Shao S, Gao Z, Yang J, Li S (2020) Active disturbance rejection control of torsional plant with unknown frequency harmonic disturbance. *Control Engineering Practice* 100: 104413.

Mohsen E, Brown LJ, Chen J (2017) A Real time Alternative to the Hilbert Huang Transform Based on Internal Model Principle. *J Electr Electron Syst* 6(233): 2332–0796.

Pigg S, Bodson M (2009) Adaptive algorithms for the rejection of sinusoidal disturbances acting on unknown plants. *IEEE Transactions on Control Systems Technology* 18(4): 822–836.

Pigg S, Bodson M (2011, June) A new algorithm for frequency estimation and disturbance cancellation inspired from induction machine theory. In *Proceedings of the 2011 American Control Conference*, 3018–3023. IEEE.

Pigg S, Bodson M (2013) Adaptive harmonic steady-state disturbance rejection with frequency tracking. *Asian Journal of Control* 15(1): 1–10.

Riviere CN, Rader RS, Thakor NV (1998) Adaptive cancelling of physiological tremor for improved precision in microsurgery. *IEEE Transactions on Biomedical Engineering* 45(7): 839–846.

Sharma PK, Sindekar AS (2016, December) Performance analysis and comparison of BLDC motor drive using PI and FOC. In *2016 International Conference on Global Trends in Signal Processing, Information Computing and Communication (ICGTSPICC)*, 485–492. IEEE.

Veluvolu KC, Tan UX, Latt WT, Shee CY, Ang WT (2007, August) Bandlimited multiple fourier linear combiner for real-time tremor compensation. In *2007 29th Annual International Conference of the IEEE Engineering in Medicine and Biology Society*, 2847–2850. IEEE.

Wen X, Yan P (2020) Disturbance-prediction–based control of input time delay systems for rejection of unknown frequency disturbances. *International Journal of Robust and Nonlinear Control* 30(1): 338–350.

Zhou Y, Jenkins ME, Naish MD, Trejos AL (2016, August) Design and validation of a high-order weighted-frequency fourier linear combiner-based Kalman filter for parkinsonian tremor estimation. In *2016 38th Annual International Conference of the IEEE Engineering in Medicine and Biology Society (EMBC)*, 5893–5896. IEEE.

Zhou Y, Jenkins ME, Naish MD, Trejos AL (2016, February) The measurement and analysis of Parkinsonian hand tremor. In *2016 IEEE-EMBS International Conference on Biomedical and Health Informatics (BHI)*, 414–417. IEEE.
Zhou Y, Jenkins ME, Naish MD, Trejos AL (2018, August) Development of a wearable tremor suppression glove. In *2018 7th IEEE International Conference on Biomedical Robotics and Biomechatronics (Biorob)*, 640–645. IEEE.